Title

A selective jumonji H3K27 demethylase inhibitor modulates the proinflammatory macrophage response

Journal

Nature, 488(7411)

ISSN

0028-0836

Authors

Kruidenier, Laurens
Chung, Chun-wa
Cheng, Zhongjun
et al.

Publication Date

2012-08-01

DOI

10.1038/nature11262

Peer reviewed

Published in final edited form as:

Nature. 2012 August 16; 488(7411): 404–408. doi:10.1038/nature11262.

A selective jumonji H3K27 demethylase inhibitor modulates the proinflammatory macrophage response

Laurens Kruidenier[1], **Chun-wa Chung**[2], **Zhongjun Cheng**[3], **John Liddle**[1], **KaHing Che**[4,5], **Gerard Joberty**[6], **Marcus Bantscheff**[6], **Chas Bountra**[4], **Angela Bridges**[2], **Hawa Diallo**[1], **Dirk Eberhard**[6], **Sue Hutchinson**[2], **Emma Jones**[2], **Roy Katso**[2], **Melanie Leveridge**[2], **Palwinder K. Mander**[1], **Julie Mosley**[2], **Cesar Ramirez-Molina**[1], **Paul Rowland**[2], **Christopher J. Schofield**[4], **Robert J. Sheppard**[1], **Julia E. Smith**[1], **Catherine Swales**[5], **Robert Tanner**[2], **Pamela Thomas**[2], **Anthony Tumber**[4], **Gerard Drewes**[6], **Udo Oppermann**[4,5], **Dinshaw J. Patel**[3], **Kevin Lee**[1,†], and **David M. Wilson**[1]

[1]Epinova DPU, Immuno-Inflammation Therapy Area, GlaxoSmithKline R&D, Medicines Research Centre, Gunnels Wood Road, Stevenage SG1 2NY, UK.

[2]Platform Technology and Science, GlaxoSmithKline R&D, Medicines Research Centre, Gunnels Wood Road, Stevenage SG1 2NY, UK.

[3]Memorial Sloan-Kettering Cancer Center, 1275 York Avenue, New York, New York 10065, USA.

[4]Structural Genomics Consortium, University of Oxford, Old Road Campus, Roosevelt Drive, Headington OX3 7DQ, UK.

[5]Botnar Research Centre, NIHR Biomedical Research Unit, University of Oxford OX3 7LD, UK.

[6]Cellzome AG, Meyerhofstrasse 1, 69117 Heidelberg, Germany.

Abstract

The jumonji (JMJ) family of histone demethylases are Fe^{2+}- and α-ketoglutarate-dependent oxygenases that are essential components of regulatory transcriptional chromatin complexes[1–4]. These enzymes demethylate lysine residues in histones in a methylation-state and sequence-specific context[5]. Considerable effort has been devoted to gaining a mechanistic understanding of the roles of histone lysine demethylases in eukaryotic transcription, genome integrity and epigenetic inheritance[2,4,6], as well as in development, physiology and disease[3,7]. However, because of the absence of any selective inhibitors, the relevance of the demethylase activity of JMJ enzymes in regulating cellular responses remains poorly understood. Here we present a

Correspondence and requests for materials should be addressed to D.M.W. (david.m.wilson@gsk.com)..
†Present address: Pfizer, Biotherapeutics R&D, 200 Cambridgepark Drive, Cambridge, Massachusetts 02140, USA.

Author Contributions L.K., C.-w.C., J.L., Z.C., G.D., U.O., D.J.P., K.C., K.L. and D.M.W. defined the research, interpreted the data and wrote the manuscript. All authors performed the experiments, analysed the data and/or contributed to the scientific discussion.

Author Information Crystal structures of JMJD3 have been deposited in the Protein Data Bank under accession numbers 4EZ4 (mouse JMJD3–NOG–Ni^{2+}), 4EYU (mouse JMJD3–NOG–Ni^{2+}), 4EZH (mouse JMJD3–H3K27me3–Ni^{2+}), 2XUE (human JMJD3–α-ketoglutarate–Fe^{2+}) and 4ASK (human JMJD3–GSK-J1–Co^{2+}). The authors declare no competing financial interests. Readers are welcome to comment on the online version of this article at www.nature.com/nature.

Supplementary Information is linked to the online version of the paper at www.nature.com/nature.

structure-guided small-molecule and chemoproteomics approach to elucidating the functional role of the H3K27me3-specific demethylase subfamily (KDM6 subfamily members JMJD3 and UTX)[8]. The liganded structures of human and mouse JMJD3 provide novel insight into the specificity determinants for cofactor, substrate and inhibitor recognition by the KDM6 subfamily of demethylases. We exploited these structural features to generate the first small-molecule catalytic site inhibitor that is selective for the H3K27me3-specific JMJ subfamily. We demonstrate that this inhibitor binds in a novel manner and reduces lipopolysaccharide-induced proinflammatory cytokine production by human primary macrophages, a process that depends on both JMJD3 and UTX. Our results resolve the ambiguity associated with the catalytic function of H3K27-specific JMJs in regulating disease-relevant inflammatory responses and provide encouragement for designing small-molecule inhibitors to allow selective pharmacological intervention across the JMJ family.

Initially, we applied a structure–function approach to elucidate the underlying recognition principles that account for the exquisite specificity of JMJD3 for H3K27me3 (trimethylated lysine 27 on histone 3) over other histone peptides containing the common ARKS amino acid motif[9]. We solved high-resolution crystal structures of the approximately 500 carboxy-terminal amino acids of mouse and human JMJD3 in the presence of cofactor and metal (Fig. 1a, Supplementary Fig. 1a and Supplementary Tables 1 and 2). The orthologue structures superimpose well on each other. The crystal structure of the histone H3(20–34)K27me3 peptide bound to an engineered mouse JMJD3 construct in the presence of the cofactor analogue *N*-oxalylglycine (NOG) and metal (Ni^{2+}) at 2.5 Å resolution is shown in Fig. 1b. This truncated JMJD3 protein encompasses residues 1,157 to 1,641 and includes a cleaved insertion segment that replaces a disordered loop, to facilitate crystal packing and peptide binding (Supplementary Fig. 2a, b).

The JMJD3 enzyme is composed of a JmjC catalytic domain and a C-terminal segment within which is embedded a Zn^{2+}-coordinated GATA-like (GATAL) domain of novel topology that is flanked by α-helical segments that form a four-helix bundle (Fig. 1b and Supplementary Fig. 1b, c). The two domains pack against each other with a large buried surface area (4,115 $Å^2$), explaining the requirement for the C-terminal domain for optimal stability and catalytic competence of the truncated JMJD3 protein (Supplementary Fig. 3).

The H3K27me3 peptide binds in a channel within the catalytic domain and amino acid residues A24 to G34 make several hydrogen-bonding and van der Waals interactions with the enzyme as is evident in Fig. 1c (see also Supplementary Fig. 4). The K27me3 group inserts deep into the catalytic pocket, bringing it close to the NOG and Ni^{2+} that lie at its base (Fig. 1d). The hydrogen-bonding interactions that anchor the H3K27 residue are shown in Supplementary Fig. 5a. The methylene side chain of K27me3 forms hydrophobic contacts with M1373. Elsewhere, the catalytic pocket is lined with polar residues: asparagine, glutamine, serine and tyrosine. The structure shows that the histone peptide residues both amino- and C-terminal to K27, especially P30 and R26, make several interactions (such as with R1246, P1388 and E1244 of JMJD3) that are important for specificity and recognition.

Both H3K9 and H3K27 have a common ARKS sequence context. It has been shown that H3K9me2 and H3K27me3 peptides bind with the same directionality to KDM7A, a dual-

specificity H3K9/H3K27 demethylase from *Caenorhabditis elegans*[9] (Supplementary Fig. 6a, b). The present study shows that the H3K27me3 peptide binds to the H3K27-specific demethylase JMJD3 in the opposite orientation to KDM7A. In part, this difference is associated with P30, which points inwards in the complex with JMJD3 but outwards in the complex with KDM7A (Supplementary Fig. 6b, c). In addition, a comparison of intermolecular contacts in our H3K27me3–JMJD3 structure with the corresponding structures of H3K9me2–PHF8 (ref. 10) and H3K9me3–JMJD2A[11,12] establishes that residues outside the ARKS segment also contribute to substrate specificity (Supplementary Fig. 7).

To understand the substrate recognition and to determine the impact on lysine demethylase activity, we mutated key residues of the H3K27me3 peptide–enzyme complex, as determined from the crystal structure (Supplementary Figs 8 and 9). In the bound state of the H3 peptide, R26 forms hydrogen bonds directly with E1244 and D1333 (Fig. 1c). The importance of these hydrogen bonds is shown by the lack of substrate turnover of the R26A mutant peptide, in which the arginine at position 26 has been replaced with alanine (Fig. 1e and Supplementary Fig. 8). Mutation of the P30 residue of H3, which is directed towards P1388 of JMJD3 (Fig. 1c), to glycine, serine or phenylalanine resulted in a loss of activity (Fig. 1e). The P30A mutant retained activity, highlighting the requirement for an appropriate hydrophobic interaction with P1388 (Fig. 1e). It has been observed that serine/threonine kinases such as MSK1 can phosphorylate H3S28 (ref. 13). Interestingly, JMJD3 did not demethylate the H3K27me3 peptide when it was phosphorylated at S28 (H3K27me3S28ph) (Supplementary Fig. 9). Our findings also indicate that the JMJD3 residues E1244, R1246, D1333 and P1388 are likely to be important for substrate recognition, as single mutations of these residues to alanine caused a loss of lysine demethylation activity. Structural and sequence comparisons of JMJD3, UTX and UTY suggest that these recognition determinants are preserved within the KDM6 subfamily of demethylases[14] (Supplementary Figs 10–12).

We exploited these structural insights, in particular the protein interactions made by α-ketoglutarate and the P30 residue of the H3 peptide, to optimize a series of weakly active hits discovered from a screening of the GlaxoSmithKline corporate compound collection (~2 million compounds[15]). The resultant lead, GSK-J1, had a half-maximum inhibitory concentration (IC_{50}) of 60 nM in the JMJD3 AlphaScreen assay (Fig. 2a). A 1.8 Å co-crystal structure of GSK-J1 bound to human JMJD3 revealed the critical interactions within the active site (Fig. 2b, Supplementary Table 2 and Supplementary Fig. 13 (omit electron-density map)). The propanoic acid of GSK-J1 mimics α-ketoglutarate binding by maintaining interactions with K1381, T1387 and N1480 (Fig. 2b and Supplementary Fig. 14a). The aromatic ring of the tetrahydrobenzazepine of GSK-J1 sits in a narrow cleft between R1246 and P1388 (Fig. 2b and Supplementary Fig. 14b), mimicking P30 of the histone peptide. GSK-J1 is competitive with α-ketoglutarate but non-competitive with the peptide substrate. This finding suggests that GSK-J1's mechanism does not follow a simple random model for bisubstrate inhibition[16] (Supplementary Fig. 15).

The pyridyl-pyrimidine biaryl of GSK-J1 makes a bidentate interaction with the catalytic metal (Fig. 2b) and induces a shift in the Co^{2+} ion (used in this crystallization experiment to

mimic the Fe^{2+} ion) of 2.34 Å away from the conserved HHE triad (Supplementary Fig. 16). Uniquely, this movement results in the metal cation swapping position with a previously apical water molecule. Subsequently, H1470 makes an indirect water-bridged interaction with the metal, whereas the direct interactions of the metal with H1390 and E1392 are preserved through small changes in their side-chain conformations (Fig. 2c and Supplementary Fig. 14c). The discovery of this subtle but distinctive dynamic metal shift in JMJD3 provides a further opportunity to derive selectivity by designing compounds that take advantage of this elasticity (Supplementary Fig. 17 and Supplementary Information (Materials)).

The overlay of the peptide and inhibitor complexes (Fig. 2c and Supplementary Fig. 18) highlights the shift in the divalent cation, as well as the overlap between bound GSK-J1 and the NOG binding site, thereby accounting for cofactor displacement in the inhibitor complex and the observed mechanism of action.

GSK-J1 is selective for the H3K27 demethylases JMJD3 and UTX and is inactive against a panel of demethylases of the JMJ family, as measured by a combination of thermal shift, mass spectrometry[17] and antibody-based assays[18] (Fig. 3a, b, Supplementary Fig. 19 and Supplementary Table 3). GSK-J1 also did not significantly inhibit 100 protein kinases at a concentration of 30 μM in a competition-binding assay (Supplementary Table 4) and had negligible off-target activity against a panel of 60 unrelated proteins, including other chromatin-modifying enzymes such as histone deacetylases (Supplementary Table 5).

The bidentate interaction between GSK-J1 and the catalytic metal is critical for enzyme inhibition. The pyridine regio-isomer GSK-J2 (Fig. 2a) cannot form such an interaction and hence showed considerably weaker JMJD3 inhibition (IC_{50} > 100 μM, Supplementary Table 3). Because GSK-J2 has analogous physicochemical properties to GSK-J1 but lacks H3K27 demethylase activity, it provides an ideal inactive control molecule for elucidating the functional role of JMJD3 inhibition.

Given the unusual binding mode of GSK-J1, we investigated its selectivity and its ability to engage full-length JMJD3 and UTX in an endogenous cellular environment by using a chemoproteomics approach. This approach combines a competition-binding assay in a cell extract, using an immobilized analogue of the inhibitor, with western blotting and mass spectrometry analysis[19]. The co-crystal structure of GSK-J1 with JMJD3 indicated that substitution at the *para* position to the pyridine nitrogen would enable access to solvent and would hence be amenable to immobilization, yielding GSK-J3 (Fig. 3c). GSK-J3 retained good activity against JMJD3 and was attached to sepharose beads to generate a KDM6 probe matrix. This matrix precipitated Flag-tagged full-length JMJD3 and UTX from transiently transfected HEK-293 cells (Fig. 3d). This interaction with JMJD3 and UTX was specific, because the addition of free GSK-J1 to the lysate completely inhibited the binding of JMJD3 and UTX to the probe matrix (Fig. 3d). To confirm the ability of GSK-J1 to bind to endogenous JMJD3 in a relevant physiological context, we next used phorbol myristate acetate (PMA)-stimulated HL-60 monocytic cells to induce the expression of JMJD3, which was then specifically captured by the GSK-J3 probe matrix (Fig. 3e). Furthermore, in quantitative mass spectrometric experiments, JMJD3 was the only protein that was

specifically captured by the probe matrix, as indicated by the inhibition of its binding in the presence of free GSK-J1 (Fig. 3f), thus confirming the remarkable selectivity of GSK-J1 in a cellular context.

Although critical for *in vitro* binding (Fig. 2b), the highly polar carboxylate group of GSK-J1 restricts cellular permeability. Therefore, we used a pro-drug strategy, masking the polarity of the acid groups of GSK-J1 and GSK-J2 with ethyl esters and yielding GSK-J4 and GSK-J5 (Fig. 4a). These cell-penetrating esters (with *in vitro* potency in the mass spectrometry assay, IC_{50} > 50 μM) are rapidly hydrolysed by macrophage esterases, thereby generating pharmacologically relevant intracellular concentrations of GSK-J1 and GSK-J2 (Table 1). The ethyl ester pro-drug GSK-J4 was confirmed to have cellular activity in Flag–JMJD3-transfected HeLa cells, in which GSK-J4 prevented the JMJD3-induced loss of nuclear H3K27me3 immunostaining (Fig. 4b and Supplementary Fig. 20). Administration of GSK-J4 increased total nuclear H3K27me3 levels in untransfected cells (Supplementary Fig. 20c).

JMJD3 is involved in several physiological functions, including the inflammatory response[20–23]. In macrophages, JMJD3 expression is rapidly induced by proinflammatory stimuli through a nuclear factor-κB (NF-κB)-dependent mechanism, and JMJD3 is recruited to the transcription start sites (TSSs) of over 70% of lipopolysaccharide (LPS)-induced genes, where it participates directly in the transcriptional response[24,25]. Crucially, it remains unclear whether this activation of transcription is achieved through the demethylation of H3K27me3 at target gene promoters[24]. Therefore, we next examined the efficacy of GSK-J4 and GSK-J5 at inhibiting the LPS-induced response of human primary macrophages derived from healthy volunteers. Administration of GSK-J4 significantly reduced the expression of 16 of 34 LPS-driven cytokines as assessed by PCR array (Fig. 4c and Supplementary Table 6), including tumour-necrosis factor-α (TNF-α).

TNF-α is important in a variety of inflammatory disorders, prompting us to make a more detailed characterization of GSK-J4's control of this cytokine. TNF-α protein production was inhibited in a dose-dependent manner (IC_{50} of GSK-J4 for TNF-α blockade, 9 μM), whereas the inactive isomer, GSK-J5, had no effect (Fig. 4d). No interference from cellular toxicity was observed under these conditions (Supplementary Fig. 21a); upstream NF-κB signalling seemed to be intact (Fig. 4e); and neither GSK-J4 nor GSK-J5 directly affected the levels of LPS-induced JMJD3 or of LPS-independent UTX and EZH2 (Supplementary Fig. 21b). Kinetic analysis suggested that the early phases of TNF-α induction were less affected by our inhibitor than were the later phases (Supplementary Fig. 21c, d). Interestingly, short interfering RNA (siRNA)-mediated knockdown of either JMJD3 or UTX alone in human primary macrophages had no effect on TNF-α production. Under these conditions, GSK-J4 was still able to inhibit TNF-α production, suggesting redundancy within the KDM6 subfamily in the regulation of this cytokine. To mimic the pan-KDM6 activity of GSK-J4, we performed dual depletion of JMJD3 and UTX in these cells, and this depletion eliminated TNF-α production (Fig. 4f and Supplementary Fig. 22). In addition, chromatin immunoprecipitation (ChIP) studies confirmed that GSK-J4, but not GSK-J5, prevented the LPS-induced loss of H3K27me3 associated with the *TNFA* TSS and blocked the recruitment of RNA polymerase II to this locus (Fig. 4g). Neither GSK-J4 nor GSK-J5

had an effect on H3K27 methylation upstream of the *TNFA* TSS (Supplementary Fig. 23). Finally, GSK-J4, but not GSK-J5, blocked the production of TNF-α by macrophages derived from patients with rheumatoid arthritis (Supplementary Fig. 24).

Our findings provide a strategy for the rational design and characterization of catalytic site inhibitors of JMJ enzymes. Specifically, we exploited active site plasticity and targeted key substrate-binding features to identify the first series of selective H3K27 inhibitors. A chemoproteomics approach was used to assess the engagement of endogenous targets and to confirm the remarkable selectivity of the inhibitors within a relevant cellular context. By using these inhibitors, we provide clear insight into the biological relevance of the demethylase function of the KDM6 JMJ enzymes. Furthermore, we show that H3K27 demethylation and specifically JMJD3 and UTX catalytic activity are critical determinants of proinflammatory gene activation in human primary macrophages. In reporting the first selective KDM6 inhibitor, we show the relevance and tractability of demethylase inhibition, as well as indicate that the KDM6 class of proteins can be targeted by epigenetic focused drug discovery, which may have broad therapeutic application.

METHODS SUMMARY

The cloning, expression, protein purification and crystallization of mouse JMJD3(1132–1641), engineered mouse JMJD3(1157–1641)–H3, human JMJD3 and their complexes are described in the Supplementary Information. GSK-J1–GSK-J5 were synthesized as pure compounds and fully characterized as outlined in the Supplementary Information. The fluorescent thermal shift assays, AlphaScreen, and RapidFire and matrix-assisted laser desorption/ionization–time of flight (MALDI-TOF) mass spectrometric assays to measure the inhibition of histone demethylase activity and JMJ selectivity, as well as the chemoproteomics experiments to establish compound–target engagement, were carried out as described in the Supplementary Information or as previously reported[19]. The procedures for the studies in human primary macrophages, including intracellular compound quantification, quantitative PCR with reverse transcription, enzyme-linked immunosorbent assays, western blotting, siRNA-mediated knockdown of JMJD3 and UTX, and ChIP are outlined in the Supplementary Information, together with a description of the antibodies and the materials.

Supplementary Material

Refer to Web version on PubMed Central for supplementary material.

Acknowledgements

We thank the following colleagues for their help and advice in preparing the manuscript: A. Argyrou, S. Atkinson, M. Barker, M. Campbell, L. Gordon, R. Gregory, R. Grimley, P. Humphreys, P. Jeffrey, A. Kucik, B. Leavens, C. Lewis, V. Ludbrook, R. Prinjha, S. Ratcliffe, C. Sharp, D. Thomas, D. Tough and M. Woodrow. Help was also provided by N. Burgess-Brown, S. Ng, J. Dunford, A. Kawamura, N. Rose and M. Daniel. D.J.P. was supported by funds from the Starr Foundation, the Abby Rockefeller Mauze Trust and the Maloris Foundation. The Structural Genomics Consortium is a registered charity (number 1097737) that receives funds from the Canadian Institutes for Health Research, the Canada Foundation for Innovation, Genome Canada, GlaxoSmithKline, Lilly Canada, the Novartis Research Foundation, Pfizer, Takeda, the Ontario Ministry of Economic Development and Innovation, and the Wellcome Trust. This study was supported by the National Institute for Health and Research (NIHR) Biomedical Research Unit, Oxford. Thanks also to M. Boesche and the Cellzome biochemistry and mass

spectrometry teams for assistance with the chemoproteomics experiments. Finally, we acknowledge additional contributions from members of Platform Technology Sciences and the Epinova DPU and the JMJD3 programme team for supporting this research.

References

1. Mosammaparast N, Shi Y. Reversal of histone methylation: biochemical and molecular mechanisms of histone demethylases. Annu. Rev. Biochem. 2010; 79:155–179. [PubMed: 20373914]
2. Klose RJ, Zhang Y. Regulation of histone methylation by demethylimination and demethylation. Nature Rev. Mol. Cell Biol. 2007; 8:307–318. [PubMed: 17342184]
3. Shi Y. Histone lysine demethylases: emerging roles in development, physiology and disease. Nature Rev. Genet. 2007; 8:829–833. [PubMed: 17909537]
4. Trojer P, Reinberg D. Histone lysine demethylases and their impact on epigenetics. Cell. 2006; 125:213–217. [PubMed: 16630806]
5. Loenarz C, Schofield CJ. Physiological and biochemical aspects of hydroxylations and demethylations catalyzed by human 2-oxoglutarate oxygenases. Trends Biochem. Sci. 2011; 36:7–18. [PubMed: 20728359]
6. Shi Y, Whetstine JR. Dynamic regulation of histone lysine methylation by demethylases. Mol. Cell. 2007; 25:1–14. [PubMed: 17218267]
7. Pedersen MT, Helin K. Histone demethylases in development and disease. Trends Cell Biol. 2010; 20:662–671. [PubMed: 20863703]
8. Kouzarides T. Chromatin modifications and their function. Cell. 2007; 128:693–705. [PubMed: 17320507]
9. Yang Y, et al. Structural insights into a dual-specificity histone demethylase ceKDM7A from Caenorhabditis elegans. Cell Res. 2010; 20:886–898. [PubMed: 20567261]
10. Horton JR, et al. Enzymatic and structural insights for substrate specificity of a family of jumonji histone lysine demethylases. Nature Struct. Mol. Biol. 2010; 17:38–43. [PubMed: 20023638]
11. Couture JF, et al. Specificity and mechanism of JMJD2A, a trimethyllysine-specific histone demethylase. Nature Struct. Mol. Biol. 2007; 14:689–695. [PubMed: 17589523]
12. Ng SS, et al. Crystal structures of histone demethylase JMJD2A reveal basis for substrate specificity. Nature. 2007; 448:87–91. [PubMed: 17589501]
13. Gehani SS, et al. Polycomb group protein displacement and gene activation through MSK-dependent H3K27me3S28 phosphorylation. Mol. Cell. 2010; 39:886–900. [PubMed: 20864036]
14. Sengoku T, Yokoyama S. Structural basis for histone H3 Lys 27 demethylation by UTX/KDM6A. Genes Dev. 2011; 25:2266–2277. [PubMed: 22002947]
15. Gamo FJ, et al. Thousands of chemical starting points for antimalarial lead identification. Nature. 2010; 465:305–310. [PubMed: 20485427]
16. Yu M, et al. Bisubstrate inhibition: theory and application to N-acetyltransferases. Biochemistry. 2006; 45:14788–14794. [PubMed: 17144672]
17. Mackeen MM, et al. Small-molecule-based inhibition of histone demethylation in cells assessed by quantitative mass spectrometry. J. Proteome Res. 2010; 9:4082–4092. [PubMed: 20583823]
18. Sakurai M, et al. A miniaturized screen for inhibitors of Jumonji histone demethylases. Mol. Biosyst. 2010; 6:357–364. [PubMed: 20094655]
19. Bantscheff M, et al. Chemoproteomics profiling of HDAC inhibitors reveals selective targeting of HDAC complexes. Nature Biotechnol. 2011; 29:255–265. [PubMed: 21258344]
20. Lan F, et al. A histone H3 lysine 27 demethylase regulates animal posterior development. Nature. 2007; 449:689–694. [PubMed: 17851529]
21. Lee MG, et al. Demethylation of H3K27 regulates polycomb recruitment and H2A ubiquitination. Science. 2007; 318:447–450. [PubMed: 17761849]
22. Agger K, et al. UTX and JMJD3 are histone H3K27 demethylases involved in HOX gene regulation and development. Nature. 2007; 449:731–734. [PubMed: 17713478]

23. Miller SA, Mohn SE, Weinmann AS. Jmjd3 and UTX play a demethylase-independent role in chromatin remodeling to regulate T-box family member-dependent gene expression. Mol. Cell. 2010; 40:594–605. [PubMed: 21095589]

24. De Santa F, et al. Jmjd3 contributes to the control of gene expression in LPS-activated macrophages. EMBO J. 2009; 28:3341–3352. [PubMed: 19779457]

25. De Santa F, et al. The histone H3 lysine-27 demethylase Jmjd3 links inflammation to inhibition of polycomb-mediated gene silencing. Cell. 2007; 130:1083–1094. [PubMed: 17825402]

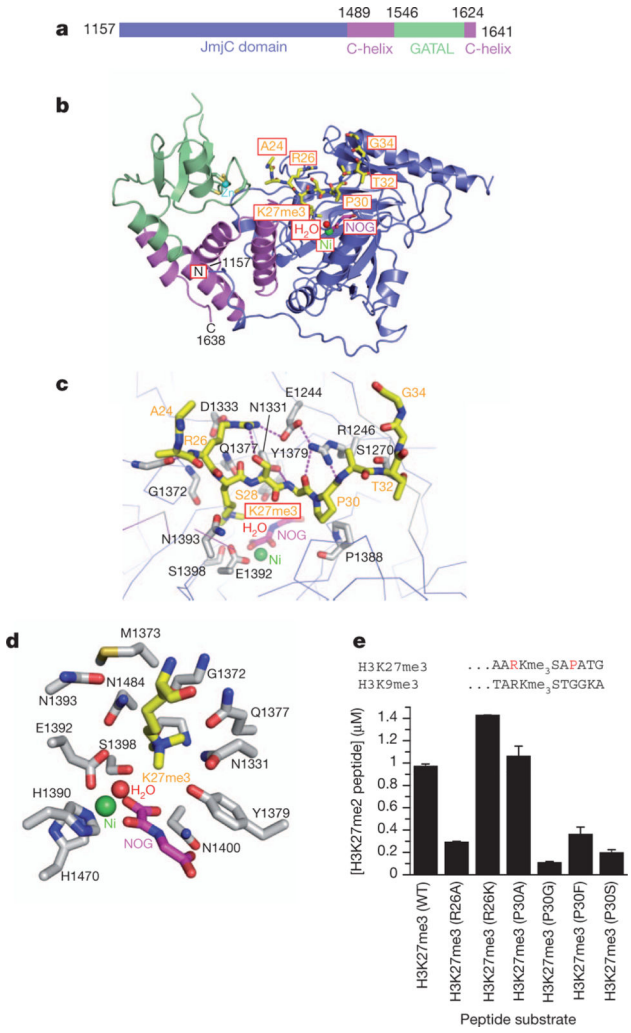

Figure 1. Structure of the H3K27me3-derived peptide bound to mouse JMJD3

a, Domain topology and numbering system of JMJD3 construct used for crystallization of the enzyme in the free state. **b**, Overview of the structure of H3(20–34)K27me3–mouse JMJD3(1157–1641) complex, with the histone peptide (K27me3, yellow) in a stick representation and the engineered enzyme (Supplementary Fig. 2) colour coded by domain as in **a**: GATAL (green), JmjC (blue) and helical (pink) domains. The heteroatoms in the stick representation are coloured according to atom type: oxygen (red) and nitrogen (blue). The N and C termini of the enzyme are indicated. **c**, View of the intermolecular interactions between the bound histone peptide (yellow) and the enzyme residues (grey), with hydrogen bonds shown as dashed pink lines. **d**, View of the catalytic pocket of the enzyme (grey), the base of which is lined by NOG (pink) and Ni^{2+} (green). The histone peptide is shown in yellow. Details of the hydrogen bonding in the catalytic pocket are outlined in Supplementary Fig. 5a. **e**, Effect of mutations of the native H3K27me3 substrate peptide (highlighted in red) at R26 and P30 on turnover. Mass spectrometric quantification of the H3K27me2 product was performed after a 6-min reaction with concentrations of peptide spanning 0.6 to 250 μM (Supplementary Fig. 8). Data are shown at approximately the K_m

(Michaelis constant) of the standard, wild-type (WT), H3K27me3 peptide (22 μM) for clarity. Data are presented as the mean ± s.d.

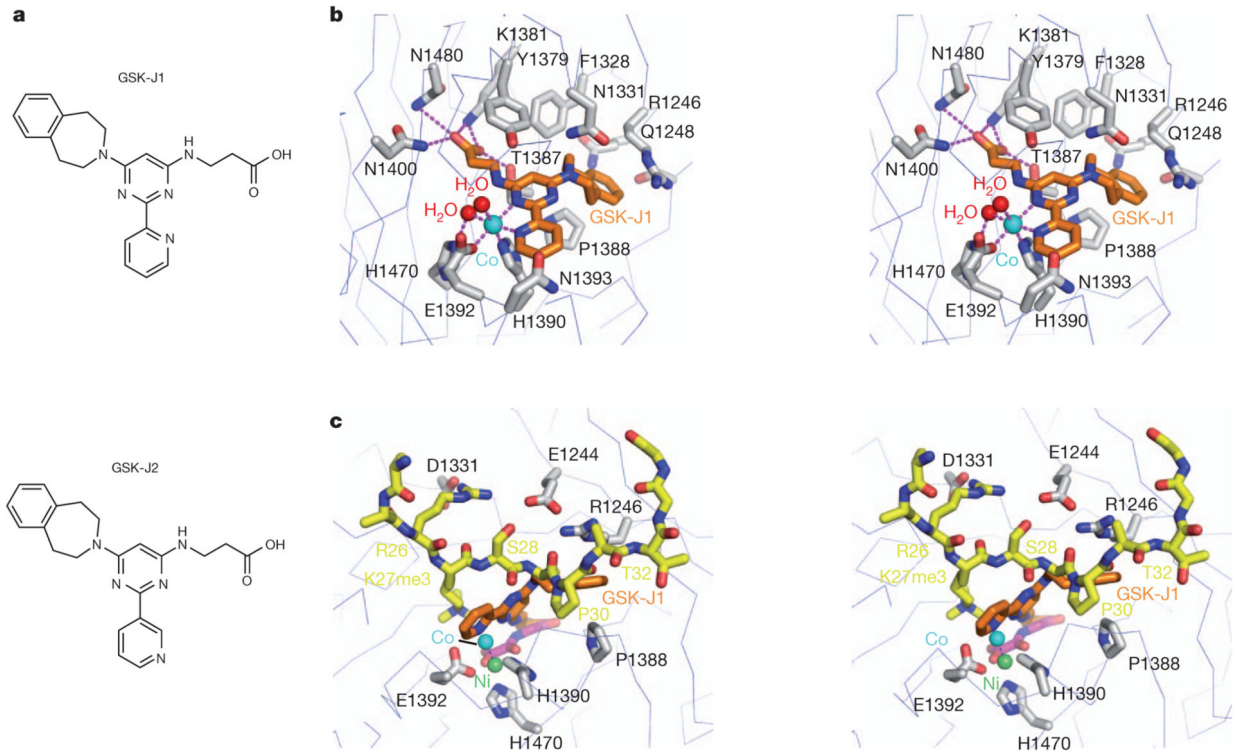

Figure 2. Structure of the inhibitor GSK-J1 bound in the catalytic pocket of human JMJD3

a, Chemical structures of GSK-J1 and GSK-J2. **b**, Stereo view of the intermolecular interactions between the bound inhibitor GSK-J1 (orange) and the human JMJD3 enzyme residues (grey) that line the catalytic pocket, with hydrogen bonds shown as dashed pink lines. The heteroatoms in the stick representation are coloured according to atom type: oxygen (red) and nitrogen (blue). **c**, Stereo view of the superposition of the bound H3K27me3 peptide and the bound inhibitor GSK-J1 in their respective complexes with JMJD3. For clarity, the histone peptide (yellow), NOG (pink), Ni^{2+} (green) and certain JMJD3 side chains (grey) are shown only from the peptide complex, and GSK-J1 (orange) and Co^{2+} (blue) are shown from the inhibitor complex.

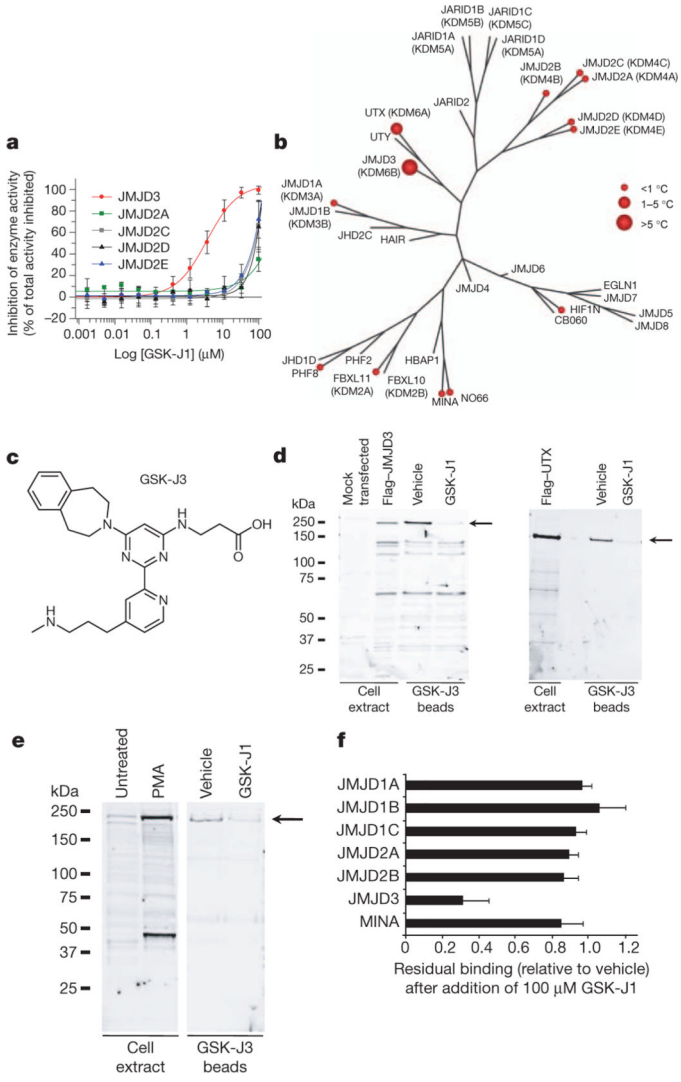

Figure 3. GSK-J1 is selective for H3K27 demethylases of the KDM6 subfamily and specifically binds to endogenous JMJD3

a, Evaluation of the selectivity of GSK-J1 in JMJ mass spectrometric assays. Data are presented as the mean ± s.d. **b**, Phylogenetic tree of human JMJ enzymes illustrating the selectivity of GSK-J1 for demethylases of the KDM6 subfamily over other KDM subfamilies of methyl-lysine demethylases, as determined by melting point (T_m) shift screening. Temperature differences (°C) are shown in red circles. Only UTX and JMJD3 show significant stabilization (>1 °C), indicating ligand binding. **c**–**f**, Chemoproteomics studies show target engagement in a cellular environment. **c**, GSK-J3, an amine analogue of GSK-J1 used for bead immobilization. **d**, Immobilized GSK-J3 was able to affinity-capture Flag-tagged JMJD3 and Flag-tagged UTX from transiently transfected HEK-293 cells. Western blotting analysis with an anti-Flag antibody shows the capture of JMJD3 (left, arrow) and UTX (right, arrow), both of which were competitively inhibited by the addition of 100 μM GSK-J1. **e**, PMA treatment of HL-60 cells (80 nM for 16 h) induced the expression of JMJD3, as shown by western blotting. Immobilized GSK-J3 captured the endogenous JMJD3 protein (arrow), and this capture was competitively inhibited by 100 μM

GSK-J1. **f**, GSK-J1 is selective for JMJD3, as shown by mass-spectrometry-based quantification of JMJC proteins (captured with GSK-J3 beads) from PMA-stimulated HL-60 cells in the presence of 100 μM GSK-J1. Data are presented as the mean from two experiments, and error bars represent the 95% confidence intervals.

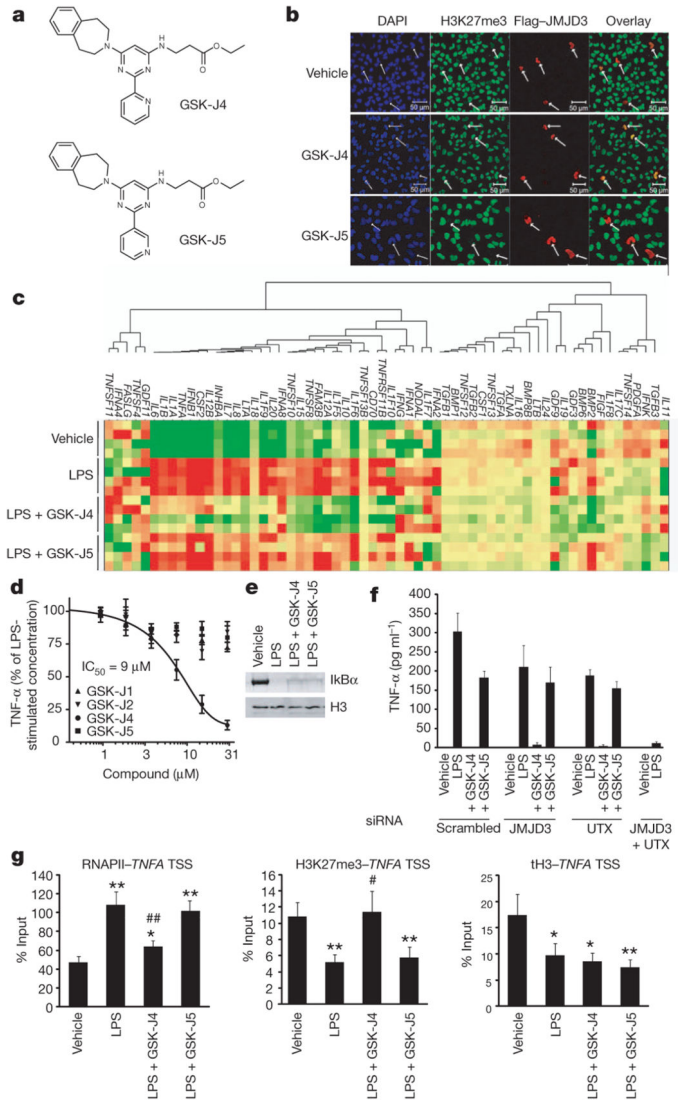

Figure 4. GSK-J1 inhibits TNF-α production by human primary macrophages in an H3K27-dependent manner

a, Chemical structures of the ethyl ester pro-drugs GSK-J4 and GSK-J5. **b**, Administration of 25 μM GSK-J4, but not GSK-J5, preserved nuclear H3K27me3 staining (green) in Flag–JMJD3-transfected (red, arrows) HeLa cells. Scale bars, 50 μm. **c**, Heat map representation of cytokine expression by human primary macrophages activated with LPS (for 2 h) in the presence of 30 μM GSK-J4 or GSK-J5 (*n* = 4 donors; green, low expression; red, high expression). **d**, TNF-α production by human primary macrophages activated with LPS in the presence of the indicated concentrations of GSK-J4 or GSK-J5 for 6 h (data are presented as the mean ± s.e.m. from *n* = 5 donors). **e**, Western blot showing the degradation of inhibitor of NF-κB α (IκBα) in whole cell lysates of LPS-stimulated human primary macrophages (30 min) in the presence of 30 μM GSK-J4 or GSK-J5. **f**, TNF-α production by LPS-stimulated human primary macrophages (1 h) transfected with scrambled, or JMJD3-directed or UTX-directed siRNA, in the presence of 30 μM GSK-J4 or GSK-J5 (data are presented as the mean ± s.d. from five transfection replicates from one representative

experiment). **g**, ChIP analysis of the association of RNA polymerase II (RNAPII), H3K27me3 and total H3 (tH3) with the *TNFA* TSS in LPS-stimulated human primary macrophages (1 h) in the presence of 30 μM GSK-J4 or GSK-J5 (data are presented as the mean ± s.e.m. from $n = 8$ donors). *P* values were calculated using a two-tailed Student's *t*-test. *, $P < 0.05$ compared with vehicle; **, $P < 0.01$ compared with vehicle; #, $P < 0.05$ compared with LPS; ##, $P < 0.01$ compared with LPS.

Table 1

Intracellular delivery of GSK-J1 and GSK-J2

Compound	[GSK-J1] in lysate (μM)	[GSK-J2] in lysate (μM)
Acid (GSK-J1 or GSK-J2)	1.6 ± 1.6	7.8 ± 1.6
Ethyl ester (GSK-J4 or GSK-J5)	11.8 ± 0.6	17.4 ± 1.5

GSK-J1 and GSK-J2 were detected in the lysates of human primary macrophages 1 h after the administration of 30 μM GSK-J1 or GSK-J2 or 30 μM of the pro-drugs GSK-J4 or GSK-J5 (mean ± s.d. from n = 3 donors).